Influence of bubbles characteristics on the skin friction and velocity gradient on solid sphere

Abdel Hafid Essadki, Iordan Nikov, Henri Delmas

Influence of Bubbles Characteristics on the Skin Friction and Velocity Gradient on Solid Sphere

A. H. Essadki,[1]* I. Nikov[2] and H. Delmas[3]

1. Ecole Supérieure de Technologie de Casablanca, B.P. 8012, Oasis, Casablanca, Morocco

2. ProBioGEM, USTL/POLYTECH'Lille, Cité Scientifique, 59655 Villeneuve d'ASCQ Cedex, France

3. Laboratoire de Génie Chimique, ENSIACET-INPT, 5 rue Paulin Talabot, 31106 Toulouse, France

A detailed study of the effects of individual bubbles at high gas flow-rate has shown, that the dominant influence on skin friction over a solid sphere is the bubble volume in compared to bubble frequency. Nevertheless the bubble frequency is very important in case of low gas flow-rate. Referring to bubbles produced by a gas distributor, statistical and spectral analyses were performed to study the influence of bubbling on exposure time and magnitude of fluctuations. Referring to a calibrated bubble train, the existence of critical frequency is demonstrated. A bubble with larger volume and a mobile, oscillatory surface generates larger velocity gradient. In the case of gas distribution, histograms of the velocity gradient for a 2 mm glass sphere creating bubble coalescence reveal the maximum exceeds 48 000 s^{-1} in the front zone and 2000 s^{-1} in the rear zone ($\theta = 180^{\circ}$). For 5 mm plastic spheres creating bubble break-up, the maximum of the velocity gradient is only 8100 s^{-1} for the front part of the sphere and 2000 s^{-1} in the rear zone.

Keywords: electrochemical probe, velocity gradient, frictional force, calibrated bubbles bubble column, statistical and spectral analysis

INTRODUCTION

Drag-velocity analysis on a particle in liquid fluidised bed system has shown that a major portion of the power draw of flow conforms to pressure drag (Nikov and Delmas, 1992). Only a small part of it, up to 20%, is due to skin friction in the external flow. However, in gas–liquid fluidised bed, the skin friction which increases rapidly with wall shear rate is related to bubble behaviour (Essadki et al., 2005). The shear rate on particles immersed in real media of food and bioproduct processing is an important component of it and should be considered. Thus, for good understanding of the role of bubbles, their properties as velocity, frequency and size have to be studied to correlate them to wall velocity gradients and the frictional force on a solid. Bakke et al. (2001) showed that operating with thin films ($<50\ \mu m$) may change the performance characteristics of the reactor. Stathopoulos and Hellums (1985) showed that microorganisms attached to microcarriers are very sensitive to excessive agitation. This may lead to biomass destruction. Croughan et al. (1987) have shown that the velocity gradient magnitude adjacent to microcarriers can be determining factors for growth. Lertpocasombut (1991) found that the biofilm thickness decreased rapidly with increasing gas velocity. Knowledge of local pressure drop by friction to the solids of a fluidised bed in columns with two- or three-phase flows allows to determining the thickness of the fixed biomass layers. In most works reported in the literature, friction is deduced from global measurements such as total pressure gradient and void fraction which may not be representative for the local conditions.

Flow complexity in two-and three-phase beds do not lead to modelling and determination of friction. However, using electrochemical spherical probe, Essadki et al. (2005) present a simple local method to obtain the velocity gradients. This work is aimed at determining to friction force and shear rate on a particle in two- and three-phase fluidised beds. The electrochemical shear-rate measurement has been validated for single-phase flow. Correlations for frictional force in fluidised beds have been worked and

*Author to whom correspondence may be addressed.
E-mail address: essadki@est-uh2c.ac.ma

recommended in cases of coalescence system and break-up systems. Vlaev et al. (2006), using the same electrochemical method, have studied the effects of rheology and impeller design on the shear field. The skin-friction drag corresponding to the impellers has been determined and compared. Yuichi et al. (2007) have studied the local skin friction profiles for individual bubbles. They concluded that the bubble size depend of the average skin friction in the intermediate bubble size condition. Groβe and Schröder (2008) have used the micropillar wall shear stress sensor to measure the dynamic wall-shear stress in turbulent pipe flow.

The present work studied the influence of individual bubbles on the frictional forces and the fluctuations of velocity gradient generated in bubble column (BC) and two- and three-phase fluidised beds.

MATERIALS AND METHODS

Experimental Apparatus

A plexiglass column of I.D. 9.4 cm and 157 cm high was employed. An electrochemical probe used as the working electrode, a nickel ring as an auxiliary electrode, and a reference electrode furnished with a Luggin's capillary were connected to potentiometer which was linked to a computer performing the acquisition of electrical current signals. Details of the apparatus have been described in a previous work (Essadki et al., 2005).

The signal has been digitised via a 12-bit UEI-800 A/D card. A home-made FORTRAN program permitted the control of data acquisition duration, frequency, statistical and spectral analysis.

Part of the column was surrounded by a square duct in order to eliminate optical distortion for visualisation. The bubbles were generated by an orifice gas distributor equipped with 1, 2 and 4 mm tubes T_1, T_2 and T_4 submerged in the liquid in the centre at the column bottom section. The tubes were placed 5 cm below the probe. The probe was placed 30 cm above the liquid distributor.

The distributor of gas was used for generating bubbles across the whole section area. It consisted of two-concentric circular tubes of 4 and 7 cm diameters with 90 regularly spaced holes (0.4 mm diameter).

Measurement of Velocity Gradient

Electrochemical technique has been adopted to measure the diffusion-limiting current, I_l, during the reduction of electroactive species (Essadki et al., 2005). The reduction occurred on a small active circular surface flush with the surface of a polymer (plastic) sphere 5 mm in diameter. The sphere was equipped with an inside channel bent 90° in which a gold wire of 1 mm diameter was introduced cut flush with the surface (Figure 1). A rigid tube served as support. The microelectrode should be positioned relative to the average direction of the main liquid flow by rotating the support. The graph 'electrical current intensity versus potential' exhibit plateau, the height of which is related to the intensity of the limiting current of the working electrode. The reduction of ferricyanide takes place at the working electrode, whereas, the oxidation of ferrocyanide takes place at the counter electrode. The physico-chemical properties of the solution are given in Table 1.

The frictional drag force was obtained by integrating the velocity gradient at the sphere surface S (Essadki et al., 2005):

$$F_f = 2\pi R^2 \eta_l \int_0^{\pi} S(\theta) \times \sin^2\theta \, d\theta \tag{1}$$

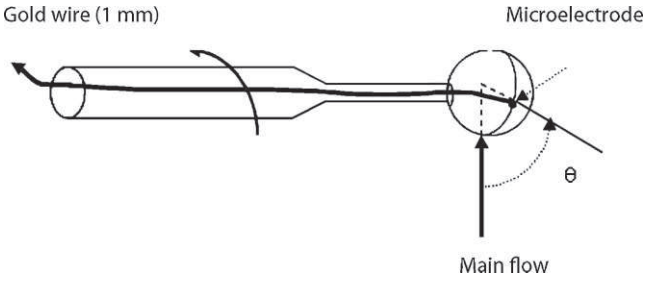

Figure 1. The electrochemical probe.

Table 1. Physico-chemical properties of the solution used in the study

Temperature (°C)	25
ρ_l ($\times 10^{-3}$ kg m^{-3})	1.0204
η_l ($\times 10^{3}$ Pa s)	1.17
D ($\times 10^{10}$ m^2 s^{-1})	5.17

The shear stress is defined by:

$\tau = \eta_l \times S$, in which η_l is the dynamic viscosity (Newtonian liquid). The apparent mass transfer coefficient K_a at any microelectrode position θ is given by:

$$K_a = \frac{I_l}{n \times F \times A_e \times C_0} \tag{2}$$

I_l is the intensity of the limiting current of the working electrode and S is related to K_a by the relationship:

$$S(\theta) = (1.16K_a)^3 \times \frac{d_e}{D^2} \tag{3}$$

D is the diffusion coefficient of the potassium ferrocyanide. D is measured by means of a turning disc using the relationship (Levart and Schumann, 1974):

$$J = D \times C_0 Sc^{1/3} \left(\frac{\omega}{\nu}\right)^{1/2} \frac{1}{k}$$
$$k = 1.61173 + 0.480306Sc^{-1/3} + 0.23393Sc^{-2/3} + 0.113151Sc^{-1} \tag{4}$$

Sc is the Schmidt number.

Signal Statistical and Spectral Analysis

A statistical analysis was applied to the temporal velocity gradient signals.

Discrete random variables can be plotted in a histogram which shows the frequency (on the ordinate) as a function of some measured parameter (on the abscissa for a given class width).

A probability density function (PDF) indicates the probability for a certain shear rate value to occur within a certain range conditions.

The relative standard deviation of the shear rate is defined as:

$$\sigma_s = \frac{\left(\overline{s^2}\right)^{1/2}}{\bar{S}} \tag{5}$$

$$\overline{s^2} = \frac{1}{T}\sum_{i=0}^{N} s^2(t_i)\ i\Delta T$$

$$S = \bar{S} + s(t)$$

$$\bar{s} = \frac{1}{T}\sum_{i=0}^{N} s(t_i)\ i\ \Delta T \tag{6}$$

ΔT is the time period acquisition time

$t_i = i*\Delta T$

The signal treatment was developed by fast Fourier transforms. These later were used to determine the power spectrum of the fluctuations of the velocity gradient, s:

$$P_s(f) = \frac{1}{T}|F_s(f)|^2 = \frac{1}{T}\left|\int_0^T s(t)\mathrm{e}^{-2\pi ift}\mathrm{d}t\right|^2 \tag{7}$$

and F_s is the Fourier transform of $s(t)$.

The aim, for a given data set of P_s computation, is intended to establish its frequency distribution and its relationship to the physical system involved.

The autocorrelation function gives evidence about the bubble passage process history and is obtained by an inverse Fourier transform, as suggested by Wiener–Kinchine theorem:

$$R(t) = \int_0^\infty P_s(f)\mathrm{e}^{2\pi ift}\mathrm{d}f \tag{8}$$

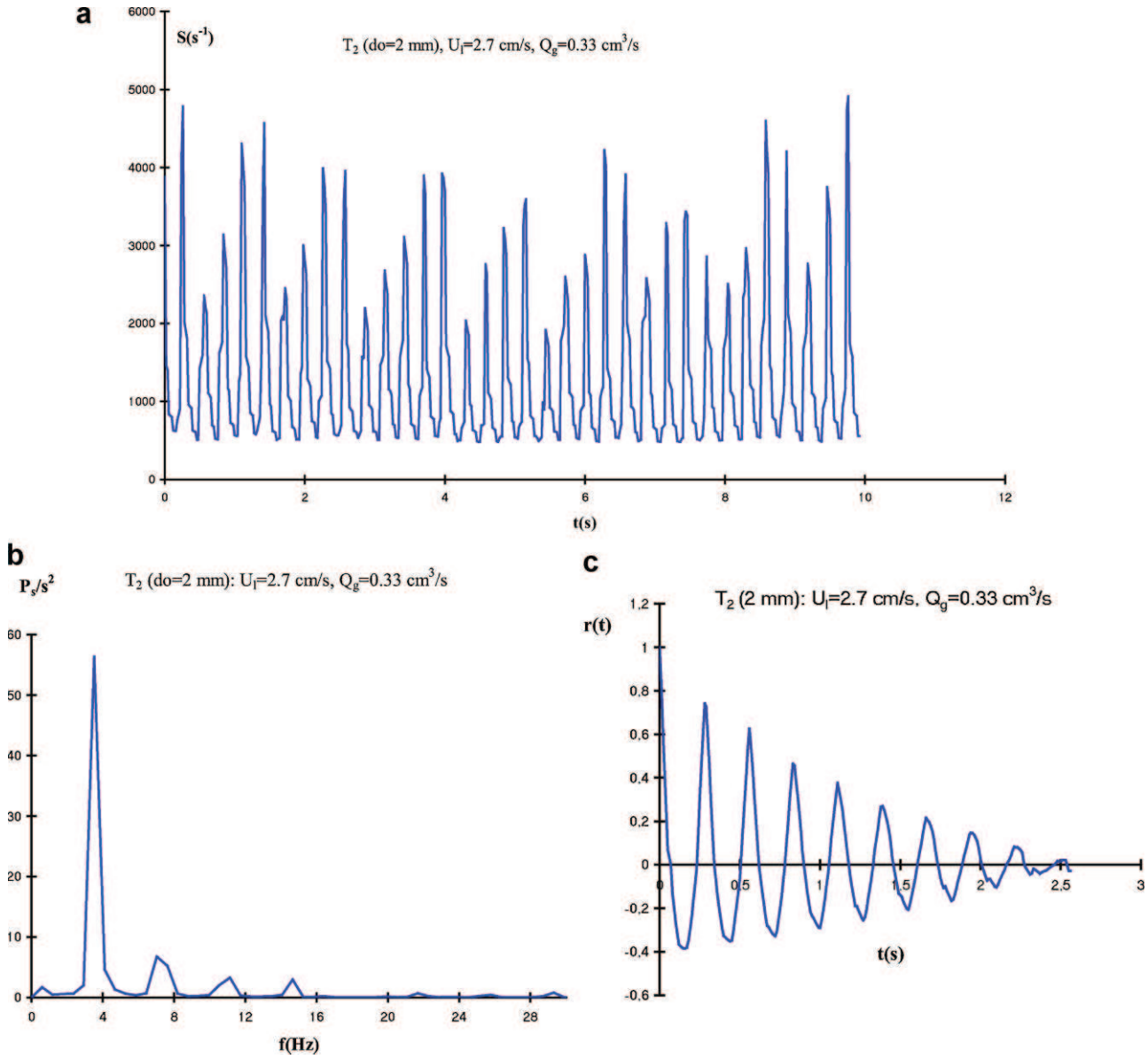

Figure 2. **a**: History records of the velocity gradient at the wall: Effect of the regular passage of bubbles near the electrochemical probe on the wall velocity gradient, $\theta = 30°$. **b**: Power spectral density function: Effect of the regular passage of bubbles near the electrochemical probe on the wall velocity gradient, $\theta = 30°$. **c**: Autocorrelation function of the velocity gradient at the wall: Effect of the regular passage of bubbles near the electrochemical probe on the wall velocity gradient, $\theta = 30°$. [Color figure can be seen in the online version of this article, available at http://onlinelibrary.wiley.com/journal/10.1002/(ISSN)1939-019X]

The normalised autocorrelation function $r(t)$ is obtained, as:

$$r(t) = \frac{R(t)}{\overline{s^2}} \tag{9}$$

To help evaluate the major frequencies in the spectrum, the average frequency of fluctuations of velocity gradient is defined, as follows:

$$\langle f \rangle = \frac{\int P_s(f) f \, \mathrm{d}f}{\int P_s(f) \, \mathrm{d}f} \tag{10}$$

The aforementioned integrals can be evaluated numerically, as:

$$\langle f \rangle = \frac{\sum P_s(f) f}{\sum P_s(f)} \tag{11}$$

All these tools allow correlation of the signal generated by the bubbles, as well as the stress distribution. The knowledge of different aspects of the signal, namely, histogram, PDF, autocorrelation, variance, etc. gives the information and uncovers the direct relationship between the signal and the prediction of shear rate or shear stress distribution.

Measurement of Volume, Velocity and Frequency of Bubbles

A high speed camera was used, for example 1000 images per second to visualise and analyse the images. It was observed that under a stationary flow-rate, the bubbles formed in line had the same shape and identical volume.

The bubble frequency was determined by counting the number of bubbles in a fixed location during of 10 s time interval, whereas, bubble rise velocity was deduced by observing the passage in locations x_1 and x_2 at time t_1 and t_2.

The bubble volume was deduced from frequency and gas flow-rate data.

$$V_b = \frac{Q_g}{f_b} \tag{12}$$

The electrochemical probe was used to measure the bubble frequency and bubble volume at low gas flow-rates (Essadki et al., 1997). Thus, the regular passage of bubbles close to the electrochemical probe at diffusionally limiting current or velocity gradient (Figure 2a) was shown on the output signal by regular spaced peaks. The frequency spectrum or the autocorrelation coefficient indicated clearly the frequency or periodicity of bubble passage. An example of the spectrum and the autocorrelation function is shown in Figure 2b and c. The comparison indicates an excellent agreement between the recording video and the electrochemical probe technique.

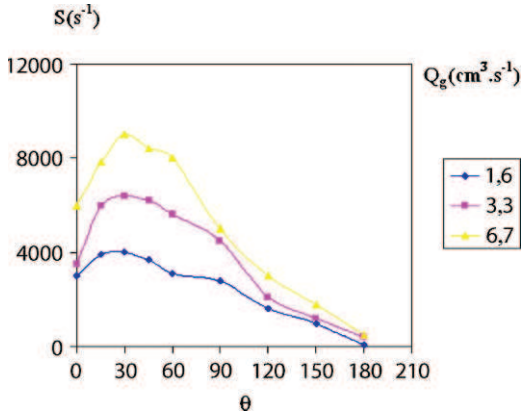

Figure 3. Velocity gradient at the wall versus θ for various gas flow-rate: Influence of calibrated bubbles generated by tube T_2 ($d_o = 2$ mm), $U_l = 6.4$ cm s^{-1}. [Color figure can be seen in the online version of this article, available at http://onlinelibrary.wiley.com/journal/10.1002/(ISSN)1939-019X]

RESULTS AND DISCUSSION

Single Orifice: Bubble Train

The average velocity gradient is deduced from the apparent mass transfer coefficient as suggested by Reiss and Hanratty (1963) for single phase.

Souhar (1979) verified that the method is valid for two-phase flow conditions if the wall was totally wetted by liquid with a film thickness of at least 20 μm. Previous experiments reported by Essadki et al. (2005) for BCs and fluidised beds showed that minimum film thickness is of about 30 μm indicating that the condition was fulfilled.

Table 2. Frictional forces on the electrochemical probe: influence of bubbles induced by different tubes diameters

Q_g (cm^3 s^{-1})[a]	0.3	1	1.6	3.3	5	6.7
V_b (cm^3)	0.055	0.062	0.055	0.064	0.122	0.175
U_b (cm s^{-1})	26.7	26.6	32.4	33.8	37.3	37.2
f_b (Hz)	6	16	30	52	41	38
$F_f \times 10^5$ (N)	8.1	14.8	18.9	19.7	23.2	28.4
Q_g (cm^3 s^{-1})[b]	0.3	1	1.6	3.3	5	6.7
V_b (cm^3)	0.11	0.198	0.155	0.208	0.199	0.202
U_b (cm s^{-1})	25.3	26.1	29.1	32.7	35.7	38.5
f_b (Hz)	3	5	11	16	25	33
$F_f \times 10^5$ (N)	5.5	8.6	16.4	27.3	28.6	38.8
Q_g (cm^3 s^{-1})[c]	0.3	1	1.6	3.3	5	6.7
V_b (cm^3)	0.165	0.25	0.21	0.24	0.29	0.32
U_b (cm s^{-1})	26.1	28.7	28.6	32	35.2	37
f_b (Hz)	2	4	8	14	17	21
$F_f \times 10^5$ (N)	4.9	10.3	16.2	27.7	32.2	39.4

[a] T_1 ($d_o = 1$ mm) and $U_l = 0.27$ cm s^{-1}.

[b] T_2 ($d_o = 2$ mm) and $U_l = 0.27$ cm s^{-1}.

[c] T_4 ($d_o = 4$ mm) and $U_l = 0.27$ cm s^{-1}.

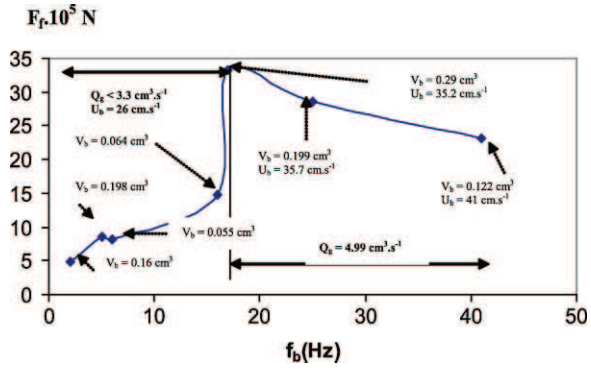

Figure 4. Frictional force versus bubble frequency for various bubble velocities and volume bubble, $U_l = 0.27\,\mathrm{cm\,s^{-1}}$. [Color figure can be seen in the online version of this article, available at http://onlinelibrary.wiley.com/journal/10.1002/(ISSN)1939-019X]

In Figure 3, the external wall velocity gradients are shown as functions of gas flow-rates corresponding to different angles between the electrode surface and the main fluid flow direction. The plots lines indicate that a clearly defined maximum obtained without gas at 45° (Essadki et al., 2005) was less accentuated with gas and the maximum was close to near 30°. The presence of bubbles has an important influence concerning the flow behaviour around the solid sphere such as drastic reduction of the wake.

The goal of the section has been targeted to study the effect of bubble characteristics such as frequency, velocity and volume. Those three parameters are most important for controlling the frictional force. The results obtained are summarised in Table 2a–c. Bubble volume and frequency were selected as independent variables and to minimise the influence of liquid velocity, this later was fixed at low value ($0.27\,\mathrm{cm\,s^{-1}}$). As shown in Figure 4 at low gas volumetric flow-rate ($Q_g < 3.3\,\mathrm{cm^3\,s^{-1}}$), inducing a bubble frequency less than 17 Hz, the influence of bubble frequency on frictional force is better pronounced than the bubble volume. For example, the frictional force created by the train of bubbles $0.2\,\mathrm{cm^3}$ at bubble frequency 5 Hz is about 8×10^{-5} N; referring to bubble volume of $0.06\,\mathrm{cm^3}$ and bubble frequency of 15 Hz, the frictional force induced is about 14×10^{-5} N.

In contrary, bubble frequency can be neglected when the gas volumetric flow-rate increases ($Q_g > 4.9\,\mathrm{cm^3}$).

In conclusion, a bubble with larger volume and a mobile, oscillatory surface generated high level of turbulence that induced high rate of liquid–solid mass transfer corresponding to high velocity gradient. The existence of a critical frequency has also been demonstrated.

Bubble Column and Fluidised Bed: Gas Distributor (Distribution)

Gas flow dynamics and solid content effect on the velocity gradient exposure

Figure 5 shows histograms of the velocity gradient in a BC at a 30° angle position, representing the sphere front corresponding to various superficial gas velocities. The liquid velocity is fixed ($U_l = 0.27\,\mathrm{cm\,s^{-1}}$). The Figure 5 shows the gradual development in gradient patterns as the gas velocity increased, the ordinate value giving the time fraction exposed to stress.

The maximum value for the velocity gradient increased steadily with gas flow.

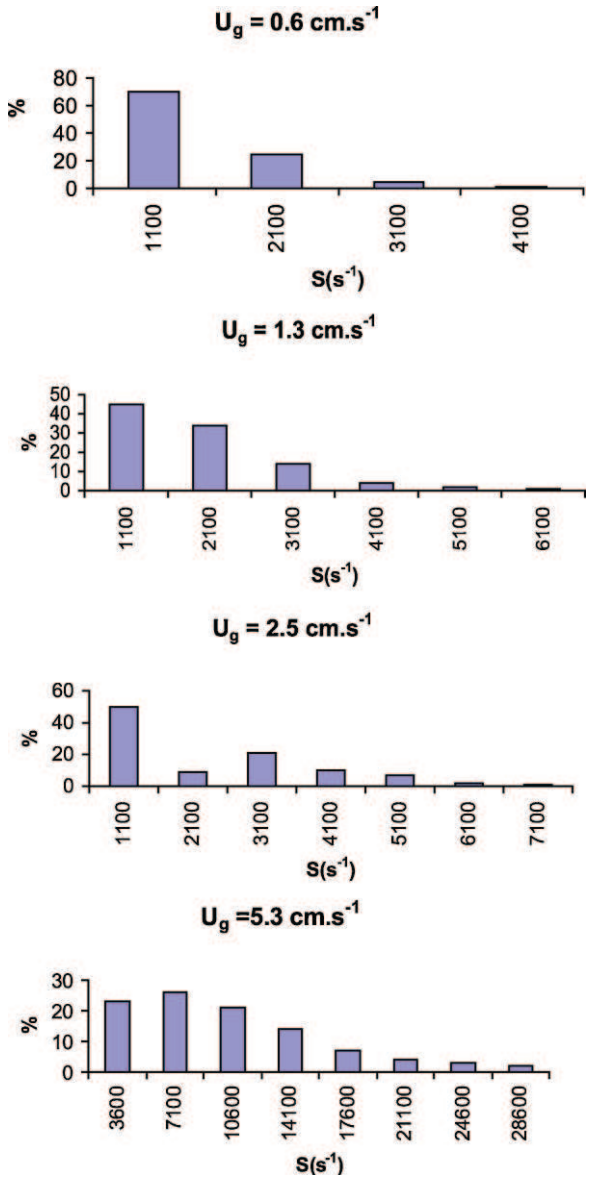

Figure 5. Histograms of the velocity gradient in bubble column (BC) at the 30° angle, $U_l = 0.27\,\mathrm{cm\,s^{-1}}$. [Color figure can be seen in the online version of this article, available at http://onlinelibrary.wiley.com/journal/10.1002/(ISSN)1939-019X]

This increase in maximum values could be attributed more to bubble-to-bubble interaction caused by the increased gas fraction and the collisions close to the probe, thus increasing local liquid shear. The maximum can reach $28\,000\,\mathrm{s^{-1}}$. In the rear zone the maximum value for $U_g = 5.3\,\mathrm{cm\,s^{-1}}$ is $2100\,\mathrm{s^{-1}}$.

Another aspect is observed in these histograms corresponding to transition bubble regime at gas velocity between 2.5 and $5.2\,\mathrm{cm\,s^{-1}}$. The maximum value in this case jumps from 7100 up to $28\,600\,\mathrm{s^{-1}}$.

In the case of fluidised bed, it is important to distinguish between a coalescence system and a break-up system. Biofilm reactors are frequently performed in fluidised or suspended bed. In this case, the decay or biomass growths are probably affected by the range of variation and the time of hydrodynamic stress exposure. In our previous work (Essadki et al., 2005), the velocity gradient and so the frictional drag force increased much more with gas velocity in the coalescence regime than in the bubble

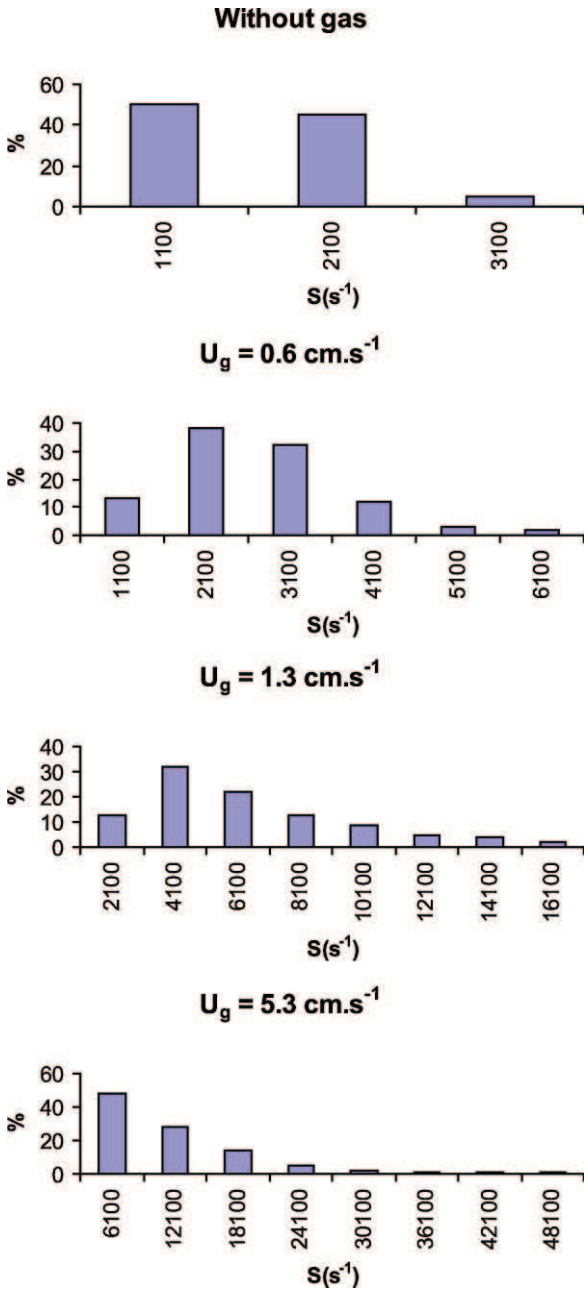

Figure 6. Histograms of the velocity gradient in fluidised bed (glass spheres, 2 mm) at the 30° angle, $U_l = 0.27$ cm s^{-1}. [Color figure can be seen in the online version of this article, available at http://onlinelibrary.wiley.com/journal/10.1002/(ISSN)1939-019X]

break-up regime. For a glass sphere of 2 mm diameter, bubble coalescence occurs, whereas, for plastic spheres of 5 mm, a bubble break-up phenomenon predominates.

The same tendency is observed for glass beads creating bubble coalescence (Figure 6) in the BC. In addition, other values of velocity gradient appear and the maximum exceeds 48 000 s^{-1} in the front zone and 2000 s^{-1} in the rear zone ($\theta = 180°$). For plastic spheres creating bubble break-up, the maximum of velocity gradient is only 8100 s^{-1} (Figure 7) for the front part of the sphere and 2000 s^{-1} in the rear zone.

The results found for both BC and fluidised bed confirm the prevalence influence of bubbles size.

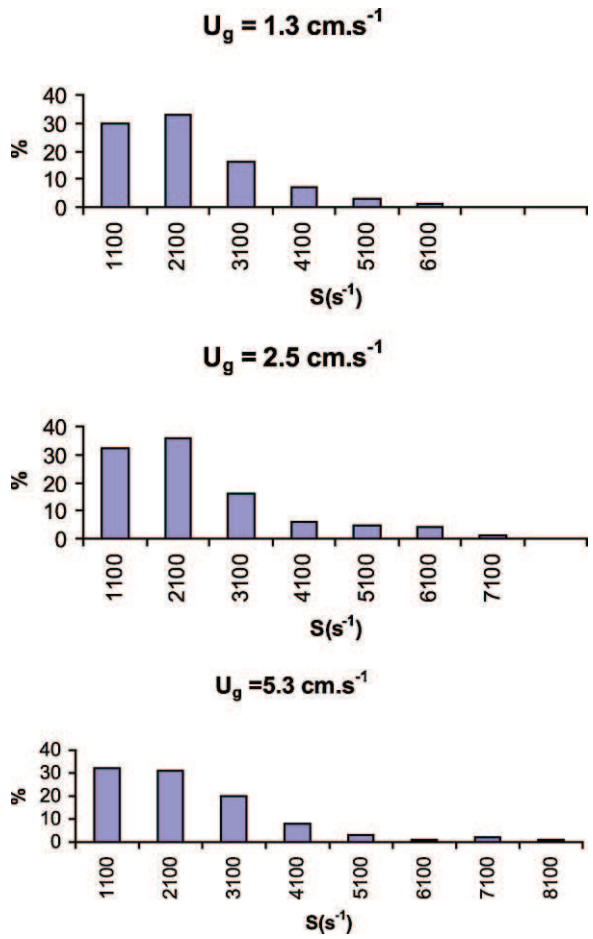

Figure 7. Histograms of the velocity gradient in fluidised bed (plastic spheres, 5 mm) at the 30° angle, $U_l = 0.27$ cm s^{-1}. [Color figure can be seen in the online version of this article, available at http://onlinelibrary.wiley.com/journal/10.1002/(ISSN)1939-019X]

Gas flow dynamics and solid content effect on relative standard deviation and fluctuation frequency of the velocity gradient

The relative standard deviation of the shear rate σ_s, shows the gas impact on the velocity gradient fluctuations which may be seen as a measure of the liquid phase turbulent fluctuations.

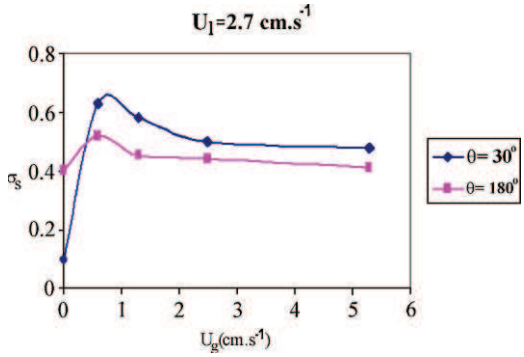

Figure 8. Relative standard deviation of the shear stress in the bubble column (BC). [Color figure can be seen in the online version of this article, available at http://onlinelibrary.wiley.com/journal/10.1002/(ISSN)1939-019X]

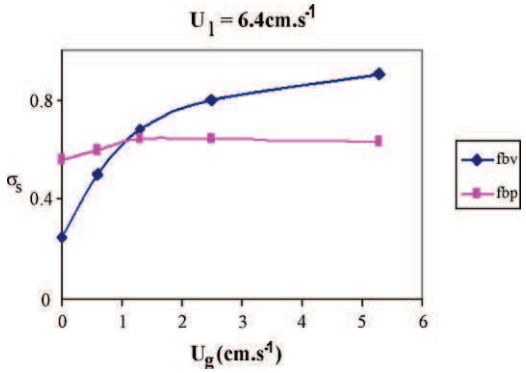

Figure 9. Relative standard deviation of the shear stress in fluidised bed. fbv, glass beads (2 mm); fbp, plastic beads (5 mm). [Color figure can be seen in the online version of this article, available at http://onlinelibrary.wiley.com/journal/10.1002/(ISSN)1939-019X]

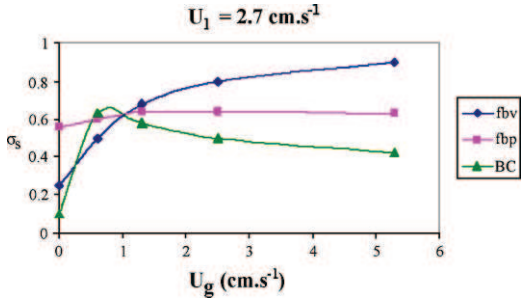

Figure 10. Relative standard deviation of the shear stress: Comparison between bubble column (BC) and fluidised (p, plastic: 5 mm; v, glass: 2 mm). [Color figure can be seen in the online version of this article, available at http://onlinelibrary.wiley.com/journal/10.1002/(ISSN)1939-019X]

In the BC, Figure 8 shows that the largest relative deviation was found at the lowest gas input. At low gas flow-rate, the large fluctuations were caused by single bubbles moving at a frequency low enough for the liquid to return to a semi-stable rest state between bubbles. At higher gas flow-rate the bubble–bubble interaction became stronger and the increase of the average velocity gradient was defined by the medium change and the increase of the maximum gradient values. It is known that, in case of a single-phase liquid, the velocity gradient fluctuations change with position on the sphere surface: the flow pattern on the front hemisphere showed a low fluctuation level, whereas, the rear zone showed higher relative fluctuation levels. With the introduction of gas, the tendency changed completely.

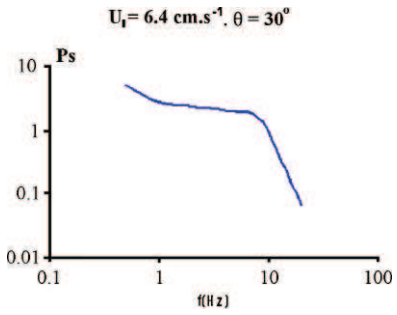

Figure 11. Typical spectrum of the three-phase fluidised bed. [Color figure can be seen in the online version of this article, available at http://onlinelibrary.wiley.com/journal/10.1002/(ISSN)1939-019X]

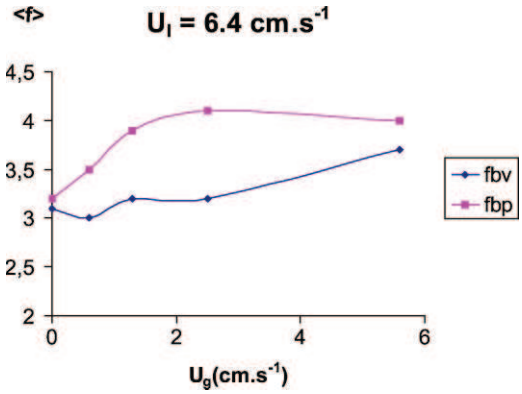

Figure 12. Average frequency of the velocity gradient at the wall in fluidised bed (p, plastic: 5 mm; v, glass: 2 mm). [Color figure can be seen in the online version of this article, available at http://onlinelibrary.wiley.com/journal/10.1002/(ISSN)1939-019X]

In the fluidised bed case, Figure 9 shows the relative fluctuation. In contrast to the case of BC, the fluidised bed showed a continuous increase in fluctuation at gas flow variation. This increase was more important in the case of glass beads creating coalescence than the plastic creating break-up in which the increase of fluctuation was very slight. The existence of large bubbles in coalescent fluidised bed occurred when the superficial gas velocity exceeded than 0.6 cm s^{-1}. This is showed by the jump in the maximum values in the histograms, for example from 6100 s^{-1} at 0.6 cm s^{-1} to 16 100 s^{-1} at 1.3 cm s^{-1} in Figure 6.

In general, the fluctuation level was found to be important in a fluidised bed than the BC (Figure 10) the reason being the presence of solids. Indeed, the solids fraction in the bed was about 0.45 giving interstitial velocities about twice as high as those in the BC and this might be the main reason for the difference.

An example of a power spectrum is given in Figure 11 for $\theta = 60^{\circ}$ for the fluidised bed without gas. The same tendency is obtained with different superficial gas velocities and both for coalescence and break-up fluidised bed. The gas influence does not appear in the spectrum which present probably the solid collisions and mask the bubbles interactions.

The average frequency is different in the cases of break-up system and the coalescence system. As expected, Figure 12 shows that the average frequency is greater in the case of plastic spheres (break-up made) than in the case of glass spheres (coalescence made).

As expected by the study of the influence of individual bubbles, the influence of bubble volume was found to be more important than bubble frequency in fluidised bed.

CONCLUSION

The study of the instantaneous local velocity gradients at the surface of fluidised particles in gas–liquid–solid flow reveal that compared to the bubble frequency bubble volume has a predominant effect. The exposure time of shear rate or shear stress shows that in coalescence regime the three-phase fluidised bed generates high values of the velocity gradient at the surface particle. In contrast to the coalescence case, the three-phase fluidised bed operating in break-up regime generates relatively low values. In both systems, the front zone of the sphere is subject to larger deformation than the rear one.

The relative standard deviation of the velocity gradient at the wall in the case of fluidised bed promoting bubble coalescence

shows that fluctuations increase with the superficial gas velocity and reaches 80%. In the case of fluidised bed promoting bubble break-up, the fluctuations remain almost constant and reach 60%. Expected, the spectral analysis confirmed that the average frequency in the 'break-up' fluidised case is greater than in the 'coalescent' fluidised case.

NOTATION

A_e	surface of microelectrode (m^2)
C_0	electroactive species concentration ($mol\,m^{-3}$)
d_o	orifice diameter (m)
d_e	microelectrode diameter (m)
D	coefficient diffusion ($m^2\,s^{-1}$)
F	Faraday constant ($A\,s\,m^{-1}$)
f	frequency (Hz)
$\langle f \rangle$	average frequency (Hz)
f_b	bubble frequency (Hz)
F_f	frictional drag force (N)
F_s	the Fourier transform of $s(t)$ (s^{-1})
I_l	intensity of diffusional-limiting current (A)
J	molar flux species ($mol\,m^{-2}\,s^{-1}$)
K_a	apparent local mass transfer coefficient ($m\,s^{-1}$)
n	number of electrons liberated during the course of the electrochemical reaction
Q_g	volumetric gas flow-rate ($m^3\,s^{-1}$)
P_s	the power spectrum of the fluctuation of the velocity gradient (s^{-1})
R	sphere radius (m)
$R(t)$	the autocorrelation function ($m^2\,s^{-2}$)
$r(t)$	the normalised autocorrelation function
S	velocity gradient at the wall (s^{-1})
$\bar{S}$	average velocity gradient at the wall (s^{-1})
s	fluctuations of the velocity gradient at the wall (s^{-1})
$\left(\overline{s^2}\right)^{1/2}$	average fluctuations of the velocity gradient at the wall (s^{-1})
Sc	Schmidt number defined by ν/D
t	time (s)
T	duration of the experiment (s)
τ	shear stress (Pa)
U_b	bubble velocity ($m\,s^{-1}$)
U_g	superficial gas velocity ($m\,s^{-1}$)
V_b	bubble volume (m^3)
U_l	superficial liquid velocity ($m\,s^{-1}$)
η_l	dynamic viscosity of liquid (Pa s)
ν	cinematic viscosity of liquid ($m^2\,s^{-1}$)
σ_s	relative standard deviation of shear rate
θ	polar angle with respect to front stagnation point
ω	angular velocity (s^{-1})

REFERENCES

Bakke, R., S. Amrani and B. Lie, "Biological nitrogen removal from wastewater; simulations and control strategies," Proceedings 42nd Conference on Simulation and Modeling; SIMS 2001, Porsgrunn, Norway (2001).

Croughan, M. S., J. F. Hamel and D. I. C. Wang, "Hydrodynamic Effects on Animal Cells Grown in Microcarrier Cultures," Biotechnol. Bioeng. **29**, 130–141 (1987).

Essadki, A. H., J. Nikov and H. Delmas, "Electrochemical Probe for Bubble Size Prediction in a Bubble Column," Exp. Therm. Fluid Sci. **14**, 243–250 (1997).

Essadki, A. H., I. Nikov and H. Delmas, "Local Shear and Skin Friction Particles in Three-Phase Fluidized Beds," Chem. Eng. Sci. **60**, 6034–6042 (2005).

Große, S. and W. Schröder, "Dynamic Measurements in Turbulent Pipe Flow Using the Micro Pillar Sensors MPS^3," Int. J. Heat Fluid Flow **29**, 830–840 (2008).

Lertpocasombut, K., "Carbon removal by thin biofilm in a three-phase fluidized bed (in French)," Thèse de Doc. Ing., INSA, Toulouse (1991).

Levart, E. and D. Schumann, "Analyse du Transport Transitoire sur un Disque Tournant en Régime Hydrodynamique Laminaire et Permanent," Int. J. Heat Mass Transfer **17**, 555–566 (1974).

Nikov, I. and H. Delmas, "Mechanism of Liquid–Solid Mass Transfer and Shear Stress in Three-Phase Fluidized Bed," Chem. Eng. Sci. **42**, 673–681 (1992).

Reiss, L. P. and T. J. Hanratty, "Experimental Study of the Unsteady Nature of the Viscous Sublayer. AIChE J. **9**(2), 154–160 (1963).

Souhar, M., "Wall friction in gas–liquid two phase flows in vertical ducts: bubble and slug regimes (in French)," Thèse Doc. Ing., INP, Nancy (1979).

Stathopoulos, N. A. and J. D. Hellums, "Shear Stress Effects on Human Embryonic Kidney Cells In Vitro," Biotechnol. Bioeng. **27**, 1021–1026 (1985).

Vlaev, S. D., I. Nikov and M. Martinov, "Shear and Skin Friction on Particles in Power-Law Fluids Agitated by Flat Blade and Fluid Foil Impellers," Chem. Eng. Sci. **61**, 5455–5467 (2006).

Yuichi, M., F. Hiroshi, O. Yoshihiko and Y. Fujio, "Skin Friction Reduction by Large Air Bubbles in a Horizontal Channel Flow," Int. J. Multiphase Flow **33**(2), 147–163 (2007).

Manuscript received June 10, 2009; revised manuscript received July 6, 2010; accepted for publication July 13, 2010.